Available online at www.sciencedirect.com
ScienceDirect
Journal of Solid State Chemistry 180 (2007) 3535–3544
JOURNAL OF SOLID STATE CHEMISTRY
www.elsevier.com/locate/jssc

Transitions between $P2_1$, $P6_3(\sqrt{3}A)$, and $P6_322$ modifications of $SrAl_2O_4$ by *in situ* high-temperature X-ray and neutron diffraction

Maxim Avdeev[a,*], Sergey Yakovlev[a], Aleksey A. Yaremchenko[b], Vladislav V. Kharton[b]

[a]*Bragg Institute, Australian Nuclear Science and Technology Organisation, 1 PBM, Menai, NSW 2234, Australia*
[b]*Department of Ceramics and Glass Engineering, CICECO, University of Aveiro, 3810-193 Aveiro, Portugal*

Received 24 August 2007; received in revised form 17 October 2007; accepted 19 October 2007
Available online 24 October 2007

Abstract

The results of *in situ* high-temperature X-ray and neutron powder diffraction experiments reconcile inconsistencies in previous reports on the symmetry of high-temperature phases of $SrAl_2O_4$. The material undergoes two reversible phase transitions $P2_1 \leftrightarrow P6_3(\sqrt{3}A)$ and $P6_3(\sqrt{3}A) \leftrightarrow P6_322$ at ~680 and ~860 °C, respectively, and the latter one is experimentally observed and characterized for the first time. The higher symmetry above the $P6_3(\sqrt{3}A) \leftrightarrow P6_322$ transition is gained by disordering off-center split site of oxygen atoms around trigonal axis rather than by unbending Al–O–Al angle to the ideal value 180°. The analysis of the literature suggests that it is a common feature of the $P6_322$ phases of stuffed tridymites.

Keywords: Stuffed tridymites; Phase transitions; X-ray diffraction; Neutron diffraction

1. Introduction

Rich crystal chemistry and a potential for application as phosphors [1] and components of composite mixed-conducting materials for ceramic membranes and fuel cells [2,3] generated significant interest in stuffed tridymite derivatives AM_2O_4 (A = Ca, Sr, Ba, Pb, Na, K; M = Al, Ga, Si, Ge, Mg, Fe, Co, Zn). Their crystal structures can be described as layers of rings of six vertex sharing MO_4 tetrahedra with A cations occupying tricapped trigonal anti-prismatic cavities. The ideal undistorted structure is described by the $P6_322$ space group with cell parameters close to those of high tridymite (A~5.2 Å, C~8.2 Å). Apical oxygen atoms linking layers, which may point either up (U) or down (D), in stuffed tridymites form UDUDUD patterns in each ring. Topologically different arrangement of tetrahedra and/or geometric distortions result in a great number of supercells and structures of lower symmetry ([4] and references therein).

In this work we focus on $SrAl_2O_4$ in order to resolve inconsistency of results reported in the literature. After the original work of Ito et al. [5] it was a common belief that the room-temperature monoclinic modification of $SrAl_2O_4$ (sp. gr. $P2_1$; a~C, b~$\sqrt{3}A$, c~A, β~93° [6]) at 650(5) °C transforms directly to the ideal hexagonal form (sp.gr. $P6_322$; a~A, c~C). In this case, according to the group-theoretical analysis recently reported by Rodehorst et al. [7], an intermediate monoclinic phase with space group $C2$ and a sequence $P2_1 \leftrightarrow C2 \leftrightarrow P6_322$ may be expected. At the same time, Fukuda et al. [8] recently observed a $\sqrt{3}A \times \sqrt{3}A \times C$ hexagonal superstructure (sp. gr. $P6_3$) by X-ray powder diffraction at 800 °C.

To rationalize the report on the transition $P2_1 \leftrightarrow P6_322$ at 650 °C [5], the observation of the phase with $P6_3(\sqrt{3}A)$ space group, i.e. having symmetry lower than $P6_322$, at 800 °C [8], and a hypothesis on the existence of the intermediate monoclinic $C2$ phase [7] we studied $SrAl_2O_4$ using *in situ* high-temperature powder diffraction. X-ray diffraction was used to follow thermal evolution of cell parameters and neutron diffraction, being much more sensitive to position of oxygen atoms, provided detailed structural information.

*Corresponding author. Fax: +61 2 9717 3606.
E-mail address: maxim.avdeev@ansto.gov.au (M. Avdeev).

0022-4596/$ - see front matter © 2007 Elsevier Inc. All rights reserved.
doi:10.1016/j.jssc.2007.10.021

2. Experimental

Polycrystalline samples of $SrAl_2O_4$ were prepared by glycine-nitrate process, a self-combustion technique using glycine as fuel and metal nitrates as oxidant [9]. In the course of synthesis, aqueous glycine-nitrate solution containing the metal cations in stoichiometric proportions was heated until self-combustion. The obtained foam-like product was ground and annealed in air at 1273 K for 2 h in order to remove organic residues. Polycrystalline samples were pressed uniaxially at 350–400 MPa and sintered in air for at 1525 °C for 10 h. The phase purity and cation composition was confirmed by X-ray powder diffraction, inductively coupled plasma spectroscopic analysis (Jobin Yvon, model JY 70 plus) and energy-dispersive spectroscopy (Rontec UHV). Equipment and procedures used for dilatometric analysis were described elsewhere [2,3].

For rather complex monoclinic modification of $SrAl_2O_4$ room temperature neutron diffraction data were collected using the high-resolution neutron powder diffractometer Echidna ($\lambda = 1.540(1)$ Å, 2Θ step 0.025°) as a part of its commissioning at the new Australian OPAL reactor. High-temperature X-ray and neutron diffraction data were collected using X′Pert Pro X-ray diffractometer equipped with Anton-Paar HTK2000 heating stage (Cu$K\alpha_{1+2}$ radiation, 2Θ step 0.017°) and the medium-resolution powder diffractometer at the HIFAR research reactor of the Australian Nuclear Science and Technology Organisation ($\lambda = 1.665(1)$ Å, 2Θ step 0.1°), respectively. Several reconnaissance X-ray experiments were carried out first to map out phase transition temperatures and the final X-ray experiment was run in the range from room temperature to 1200 °C with temperature steps as small as 2 °C in the vicinity of phase transitions. Neutron diffraction data were collected at room temperatures, 615, 710, 800, 1000 and 1200 °C for 9–22 h that provided, as we show below, two data sets in each of three phase fields. At each temperature the diffraction data were collected as a series of 1 h data sets that were found to be identical. This indicates that at each temperature step the sample reached an equilibrium state. Rietveld refinements were performed using GSAS code with EXPGUI front-end [10,11].

3. Results and discussion

3.1. Overview of the X-ray diffraction data from room temperature to 1200 °C

The room temperature X-ray powder diffraction data perfectly matched the pattern No74-794 of the PDF2 database [12] calculated from the original crystallographic data of Schulze and Müller–Buschbaum for the monoclinic phase of $SrAl_2O_4$ [6]. The subsequently collected *in situ* high-temperature X-ray powder diffraction data clearly indicated transformation of the monoclinic structure to the one with hexagonal unit cell metrics at ~680 °C in agreement with previous reports [5,7,13] (Fig. 1). However, careful examination of the diffraction data above phase transition revealed a number of reflections that are not allowed by the $P6_322$ space group (Fig. 2). The raw diffraction data indicated that these weak superstructure reflections disappear at ~860 °C and in the whole range from the hexagonal↔monoclinic transition at 680–860 °C the diffraction data were successfully indexed by the hexagonal supercell $\sqrt{3}A \times \sqrt{3}A \times C$ with space group $P6_3$. In addition to the observation of extra reflections, temperature evolution of cell parameters confirmed the

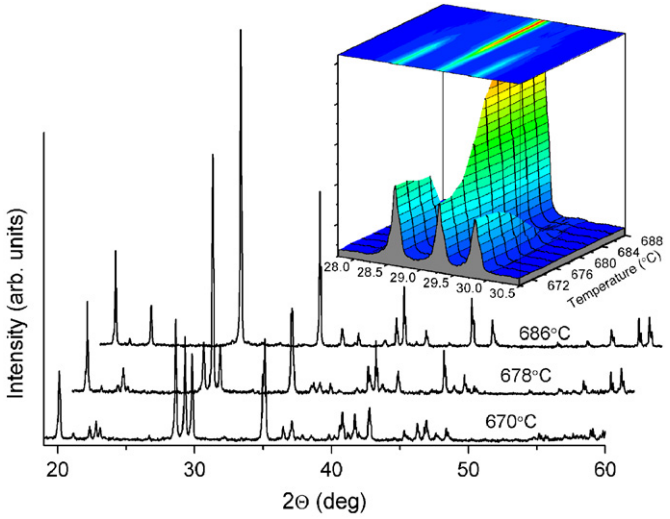

Fig. 1. Representative X-ray diffraction patterns for $SrAl_2O_4$ collected at 670, 678 and 686 °C (from bottom to top) indicating the monoclinic, monoclinic + hexagonal, and hexagonal phases respectively. Inset illustrates evolution of diffraction intensity in the characteristic region 28.5–30.5° 2Θ through the phase transition. The surface and the contour were interpolated through the series of patterns collected every 2 °C in the range of 670–688 °C.

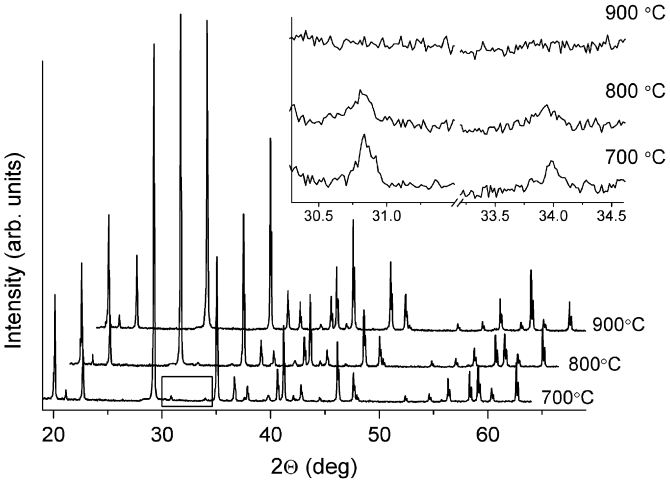

Fig. 2. X-ray diffraction data for $SrAl_2O_4$ collected at 700, 800, and 900 °C indicating hexagonal symmetry of crystal structure at all three temperatures. Inset shows extra reflections, a signature of the $P6_3(\sqrt{3}A)$ supercell, at 700 and 800 °C, but not at 900 °C.

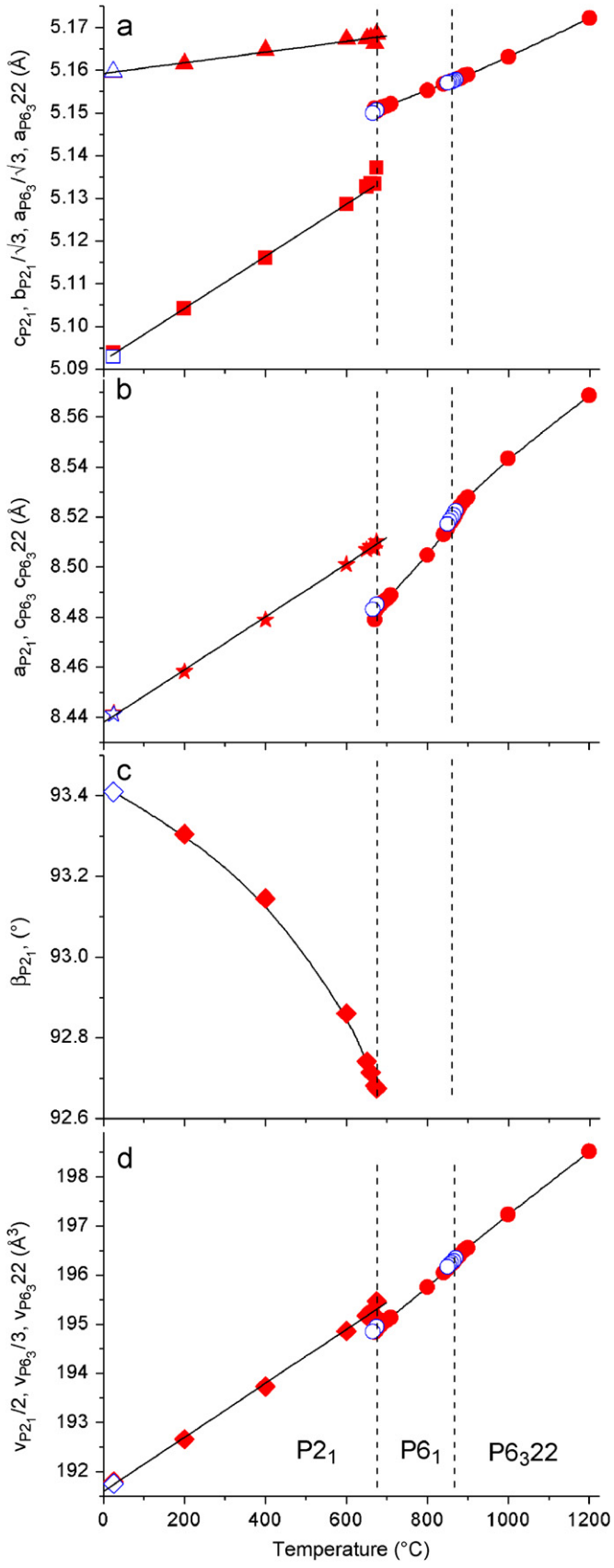

Fig. 3. Unit cell parameters of $SrAl_2O_4$ as a function of temperature from X-ray diffraction on heating (filled symbols) and cooling (open symbols). Error bars are smaller than symbols. Solid lines are guides for the eye. Dashed lines indicate stability fields of the $P2_1$, $P6_322$ and $P6_3$ phases.

existence of a second phase transition for $SrAl_2O_4$ (Fig. 3). Changes are less pronounced than those observed at ~680 °C as they are related to more subtle structural effects (see Section 3.3) but they still can be clearly seen especially by the anomaly in the behavior of the c cell parameter (Fig. 3b). The data above 860 °C were successfully indexed by the unit cell $A \times A \times C$ with space group $P6_322$.

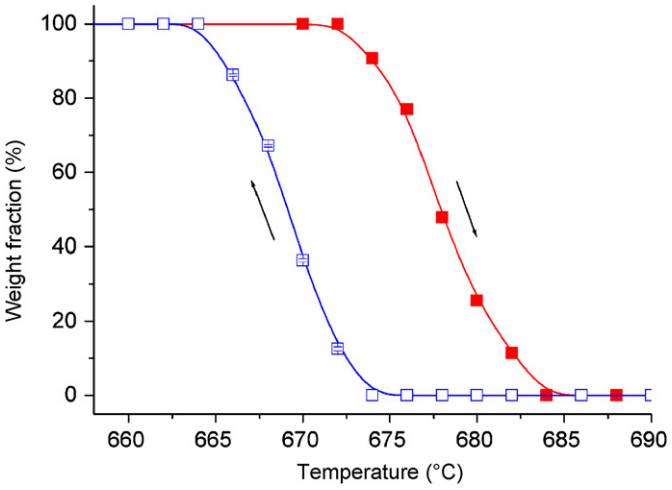

Fig. 4. Weight fraction of the monoclinic $P2_1$ modification as a function of temperature on heating (filled symbols) and cooling (open symbols) in the vicinity of $P2_1 \leftrightarrow P6_3$ phase transition.

Table 1
Monoclinic/hexagonal phase coexistence interval for $SrAl_2O_4$

Reference	Heating (°C)	Cooling (°C)
Ito et al. [5]	640(10)	
Henderson and Taylor [13]	665–705	695–655
This work	672–684	674–664

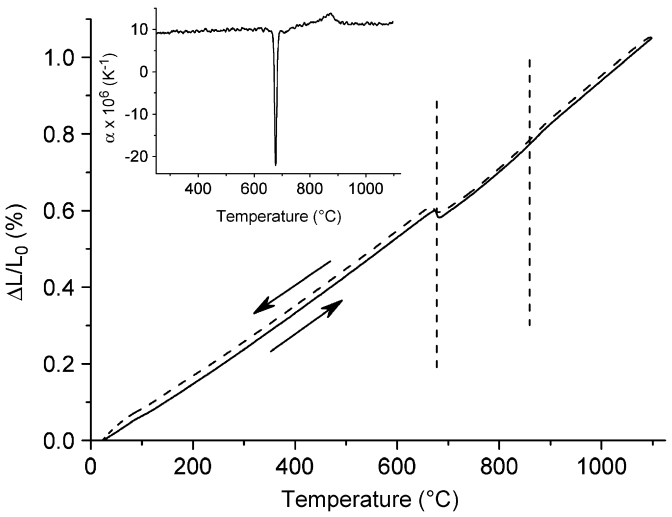

Fig. 5. Dilatometric curves for $SrAl_2O_4$ collected on heating and cooling. Inset shows thermal expansion coefficient as a function of temperature.

3.1.1. $P2_1 \leftrightarrow P6_3$ phase transition

The extra X-ray reflections indicating that the correct space group of $SrAl_2O_4$ in the region 680–860 °C is $P6_3$ are very weak and it is hardly surprising that they have been overlooked in the previous X-ray diffraction studies [5,13]. However, aside from the issue with space group assignment all other features of the monoclinic↔hexagonal phase transition for $SrAl_2O_4$ we observed are in agreement with the results reported before [13]. This includes a considerable (−0.25%) drop of cell volume on structure transformation to high-symmetry modification (Fig. 3d) and discontinuity in the evolution of monoclinic angle β which, contrary to intuitive expectations, never reaches the ideal value of 90° before the structure transforms to hexagonal symmetry (Fig. 3c). The temperature hysteresis for the transition was found to be ~9 °C and both on heating and cooling hexagonal and monoclinic phases coexist over the range of ~11 °C (Figs. 1 and 4). The values of phase transition characteristic temperatures extracted from our data analysis and from literature show some scatter (Table 1) that we attribute to the a thermal martensitic mechanism of the transition [13] and thus its sensitivity to sample microstructure, thermal history, etc.

We found no indication of the intermediate $C2$ monoclinic phase either in the raw diffraction data or in the behavior of cell parameters as a function of temperature but there is no contradiction between this fact and the proposed sequence $P6_322 \leftrightarrow C2 \leftrightarrow P2_1$ [7]. The sequence involving intermediate $C2$ monoclinic space group is only one of the possible paths from $P6_322$ to $P2_1$. Examination

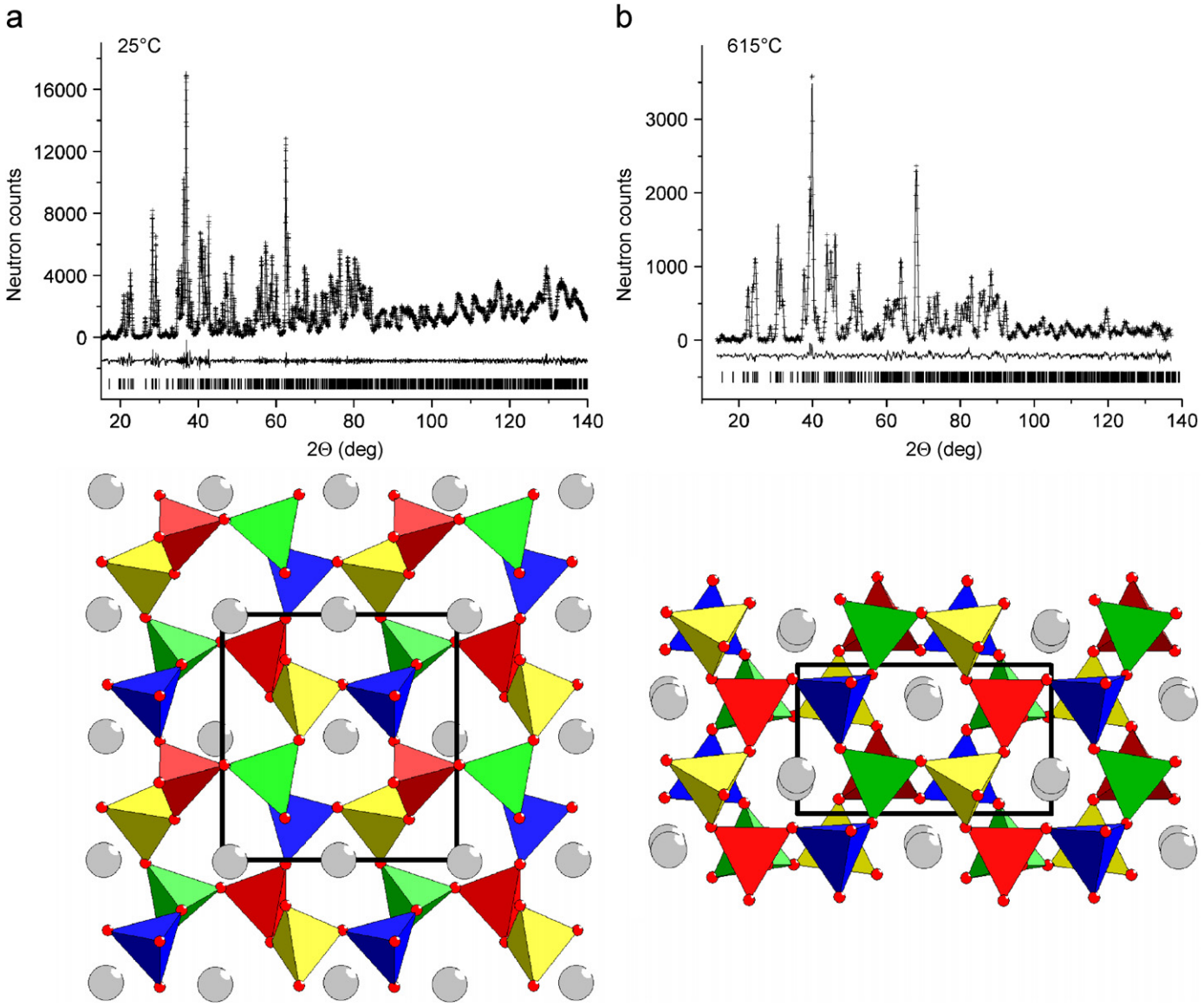

Fig. 6. Top: neutron powder diffraction observed and calculated profiles, and difference curves for the monoclinic $P2_1$ modification of $SrAl_2O_4$ at room temperature (a, high-resolution data) and at 615 °C (b, medium-resolution data). Bottom: view of $P2_1$ modification of $SrAl_2O_4$ perpendicular (left) and parallel (right) to the monoclinic a-axis (c-axis in hexagonal $P6_3$ and $P6_322$ forms). Different colors represent oxygen tetrahedra around crystallographically inequivalent Al atoms.

of group–subgroup relations for the $P6_322$ space group revealed that there is a chain consistent with the observed sequence of phase transitions, i.e. $P6_322 \rightarrow P6_3 \rightarrow P2_1$, which does not require intermediate monoclinic $C2$ group [14].

3.1.2. $P6_3 \leftrightarrow P6_322$ phase transition

It was more difficult to extract the details for the $P6_3 \leftrightarrow P6_322$ phase transition from the X-ray diffraction data as it manifests itself mainly by presence or absence of very weak superstructure reflections. Still it should be mentioned that evolution of supercell peaks intensity and unit cell metrics both changing through the transition continuously suggests its second-order nature. Careful dilatometric measurements confirmed the results of diffraction experiments, i.e. while thermal expansion of the material through the transition at 860 °C is continuous, accompanied only by change of slope, the thermal expansion coefficient demonstrates discontinuity (Fig. 5), that is a combination characteristic for second-order transitions.

Based on the results of X-ray diffraction data analysis we could draw the following preliminary conclusions:

(1) $SrAl_2O_4$ undergoes structural phase transitions at approximately 680 and 860 °C.
(2) The first-order transition at 680 °C from monoclinic to hexagonal modification was reported before [5], but the space group was assigned incorrectly. The correct space group for $SrAl_2O_4$ in the range 680–860 °C is $P6_3$ with the unit cell $\sqrt{3}A \times \sqrt{3}A \times C$. The single temperature point 800 °C at which $P6_3$ phase was observed before falls in this range and thus the report of Fukuda et al. [8] is consistent with our results.
(3) The transition $P6_3 \leftrightarrow P6_322$ at 860 °C observed for the first time appears to be of second order.
(4) The intermediate $C2$ monoclinic phase proposed to link $P2_1$ and $P6_322$ modifications [7] was not observed and that is consistent with the fact that an alternative $P2_1 \leftrightarrow P6_3 \leftrightarrow P6_322$ sequence does not require such a phase.

3.2. Neutron powder diffraction results

3.2.1. $P2_1$ phase at room temperature and 615 °C

We used the original crystallographic data of Schulze and Muller–Buschbaum [6] as a starting model for Rietveld refinement of the high-resolution neutron powder diffraction data collected for $SrAl_2O_4$ at room temperature. Following the authors, the y coordinate for the general ($2a$) site of Sr1 atom was fixed to 0. The refinement smoothly converged to the structure close to the starting model based on single-crystal X-ray diffraction data. Then the result of the room-temperature data refinement was used as a starting model for the Rietveld analysis of the medium-resolution data collected at 615 °C that also resulted in a sensible structure. The Rietveld plots and structure view for the monoclinic modification of $SrAl_2O_4$ at room temperature and 615 °C are presented in Fig. 6. The crystallographic details are provided in Table 2.

3.2.2. $P6_3$ phase at 710 and 800 °C

The neutron powder diffraction data collected at 710 and 800 °C clearly indicated the same extra reflections characteristic for the $P6_3(\sqrt{3}A)$ superstructure as the X-ray data (Fig. 7). Their intensity is more pronounced

Table 2
Structural parameters for $SrAl_2O_4$ refined from neutron powder diffraction data collected at room temperature and 615 °C using monoclinic space group $P2_1$ (No. 4) with all the atoms in general $2a(x,y,z)$ site

Atom	25 °C[a]				615 °C[b]			
	x	y	z	100 Uiso, Å^2	x	y	z	100 Uiso, Å^2
Sr1	0.4946(4)	0	0.2514(7)	0.65(8)	0.4968(7)	0	0.2530(12)	2.05(14)
Sr2	0.0315(5)	0.9922(8)	0.2024(6)	1.04(8)	0.0250(7)	0.9939(12)	0.2111(12)	3.17(17)
Al1	0.1914(11)	0.8299(11)	0.7175(15)	1.6(2)	0.193(2)	0.829(2)	0.728(3)	3.5(4)
Al2	0.8036(10)	0.8361(11)	0.7349(15)	0.4(2)	0.796(2)	0.832(2)	0.737(3)	1.3(3)
Al3	0.7082(10)	0.6680(11)	0.2239(14)	0.3(2)	0.698(2)	0.661(2)	0.226(3)	1.7(4)
Al4	0.6787(9)	0.1678(11)	0.8005(16)	0.7(2)	0.679(2)	0.171(2)	0.786(3)	1.2(3)
O1	0.2659(6)	0.1688(8)	0.4364(11)	0.94(15)	0.2613(1)	0.1707(13)	0.4320(18)	2.1(3)
O2	0.7313(6)	0.3145(8)	0.5873(7)	0.46(12)	0.7283(10)	0.3202(14)	0.5782(18)	2.9(3)
O3	0.3262(5)	0.4876(9)	0.3480(8)	0.97(10)	0.3215(8)	0.4914(17)	0.3580(13)	2.7(2)
O4	0.2674(5)	0.9826(9)	0.9008(8)	0.91(9)	0.2578(8)	0.9861(18)	0.9011(14)	3.1(2)
O5	0.1728(6)	0.2949(7)	0.9348(12)	0.96(14)	0.1871(10)	0.3034(13)	0.9307(19)	1.9(2)
O6	0.2046(6)	0.66512(7)	0.9064(9)	0.78(13)	0.2107(11)	0.6712(15)	0.922(2)	4.3(3)
O7	0.4882(6)	0.2135(7)	0.8788(10)	1.37(15)	0.4949(10)	0.2076(14)	0.871(2)	4.3(3)
O8	0.9919(6)	0.8863(7)	0.6514(10)	1.68(15)	0.9894(11)	0.8783(13)	0.6568(17)	5.0(3)

Numbers in parentheses are standard deviations of last significant digits. Values with no standard deviation shown were not refined. Atomic thermal displacement parameters values are multiplied by 100.
[a]25 °C: $a = 8.44365(9)$ Å, $b = 8.82245(8)$ Å, $c = 5.15964(6)$ Å, $\beta = 93.411(1)°$; $R_p = 4.04\%$, $R_{wp} = 2.69\%$, $\chi^2 = 3.80$.
[b]615 °C: $a = 8.5066(5)$ Å, $b = 8.8898(5)$ Å, $c = 5.1732(3)$ Å, $\beta = 92.875(4)°$; $R_p = 2.80\%$, $R_{wp} = 2.26\%$, $\chi^2 = 3.22$.

as the superstructure originates from ordered displacements of oxygen atoms (see Section 3.3) and neutron diffraction is much more sensitive to position of oxygen atoms than X-ray diffraction. As a starting model for the Rietveld analysis we used the structure of the $P6_3(\sqrt{3}A)$ phase of $BaCoSiO_4$ solved using single crystal X-ray diffraction data [15]. Following the authors [15], the z coordinate of the Sr1 atom was fixed to 0.25 in order to define the origin of the $P6_3$ space group. Since the number of variables significantly decreased compared to the monoclinic structure the data were refined with anisotropic thermal parameters for atoms with high neutron scattering lengths, i.e. Sr and O, and the results are presented in Fig. 7. The crystallographic details are provided in Table 3.

3.2.3. $P6_322$ phase at 1000 and 1200 °C

In agreement with the results of X-ray diffraction the neutron powder diffraction data collected at 1000 and 1200 °C indicated no trace of superstructure reflections (Fig. 8a and b, insets) and the pattern was successfully indexed using the basic $A \times A \times C$ hexagonal unit cell and the $P6_322$ space group. The structure of the high-temperature modification of $BaAl_2O_4$ [16] was used as a starting model for the Rietveld refinement of the data collected at 1000 °C. Initially, as a test, the apical oxygen atom was placed in the ideal $2c$ (1/3, 2/3, 1/4) site. However, the refinement resulted in the anisotropic thermal parameter with unreasonably high $U_{11}(=U_{22})$ components in the *ab*-plane and difference Fourier syntheses clearly showed 3-fold off-center site splitting

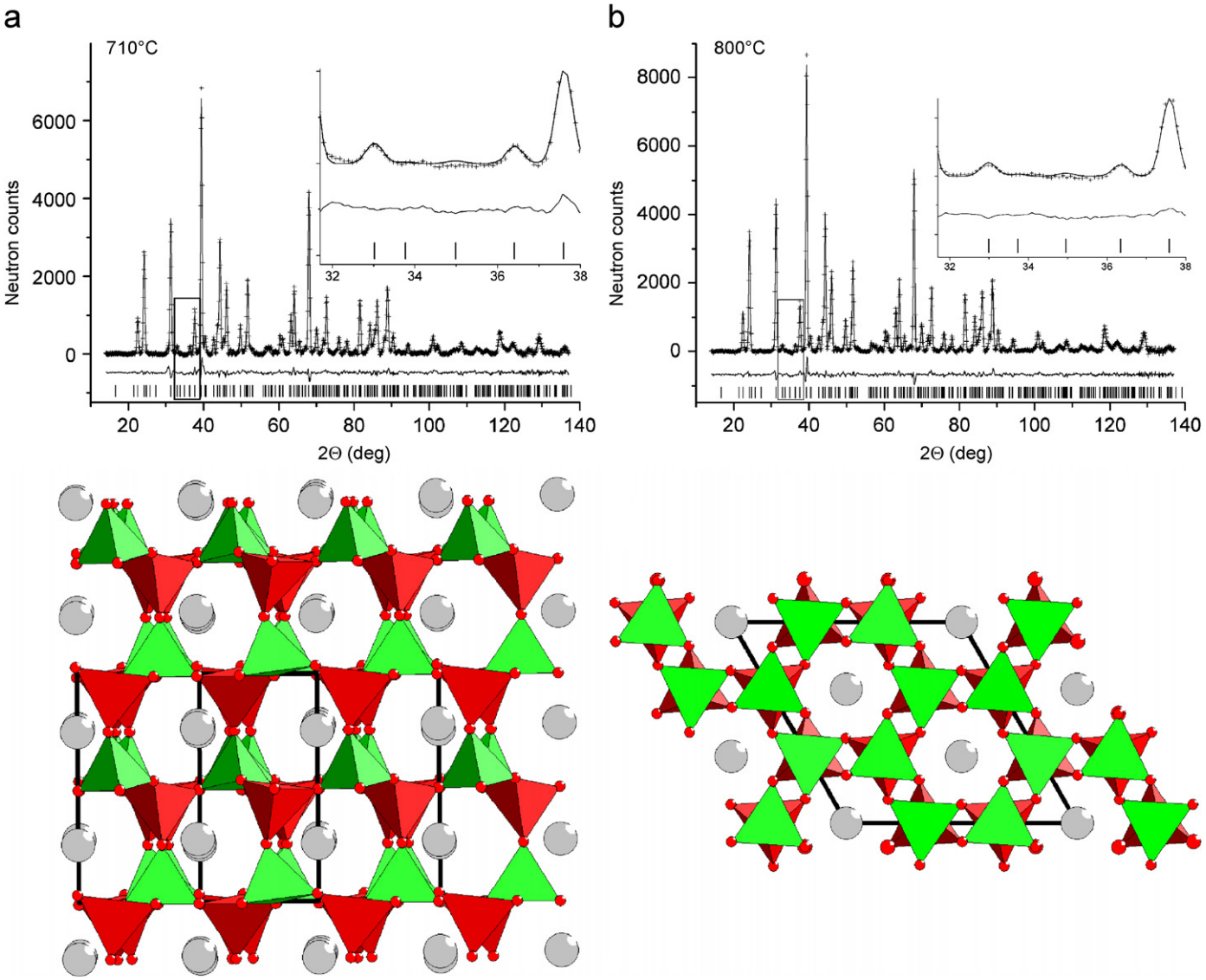

Fig. 7. Top: neutron powder diffraction observed and calculated profiles, and difference curves for the hexagonal $P6_3(\sqrt{3}A)$ modification of $SrAl_2O_4$ at 710 and 800 °C. Inset shows the same extra reflections characteristic for $P6_3$ superstructure as X-ray diffraction data (Fig. 2). The 2Θ angles of peak position differ due to the different wavelength used. Bottom: view of $P6_3$ modification of $SrAl_2O_4$ perpendicular (left) and parallel (right) to the hexagonal c-axis. Different colors represent tetrahedra of crystallographically inequivalent Al atoms.

Table 3
Structural parameters for $SrAl_2O_4$ refined from neutron powder diffraction data collected at 710 and 800 °C using hexagonal space group $P6_3$ (No. 173) with Sr1 at 2*a*(0,0,1/4), Sr2 and Sr3 at 2*b*(1/3,2/3,*z*), and Al1, Al2, and O1–O4 at 6*c*(*x*,*y*,*z*)

Atom	*x*	*y*	*z*	U_{11}, Å^2	U_{22}, Å^2	U_{33}, Å^2	U_{12}, Å^2	U_{13}, Å^2	U_{23}, Å^2
				710 °C[a]					
Sr1	0	0	1/4	5.0(9)	$= U_{11}$	15(2)	2.5(6)	0	0
Sr2	1/3	2/3	0.238(4)	3.4(5)	$= U_{11}$	2.3(8)	1.7(3)	0	0
Sr3	1/3	2/3	0.725(5)	2.6(6)	$= U_{11}$	4.8(12)	1.3(3)	0	0
Al1	0.333(4)	0.340(4)	0.548(5)			$U_{iso} = 4.0(5)$			
Al2	0.335(3)	0.341(3)	0.940(4)			$U_{iso} = 2.3(4)$			
O1	0.320(4)	0.375(3)	0.749(5)	37(2)	22(2)	4.0(5)	27(2)	−1(2)	0(2)
O2	0.118(2)	0.878(2)	0.010(4)	3.7(12)	1(1)	18(2)	−1.0(7)	4.8(12)	−1(1)
O3	0.786(2)	0.219(2)	−0.033(4)	4.6(13)	1.8(10)	23(3)	1.8(10)	−6.6(13)	−3.1(12)
O4	0.451(2)	0.547(2)	0.009(4)	3.3(12)	1.0(8)	11.2(16)	0.5(8)	1.1(11)	−1.6(11)
				800 °C[b]					
Sr1	0	0	1/4	6.1(9)	$= U_{11}$	10(2)	3.1(5)	0	0
Sr2	1/3	2/3	0.246(3)	2.8(4)	$= U_{11}$	5.2(9)	1.4(2)	0	0
Sr3	1/3	2/3	0.738(4)	2.9(5)	$= U_{11}$	6.7(10)	1.4(2)	0	0
Al1	0.330(3)	0.334(3)	0.557(4)			$U_{iso} = 5.0(4)$			
Al2	0.333(2)	0.338(2)	0.947(3)			$U_{iso} = 1.8(3)$			
O1	0.324(3)	0.378(2)	0.756(5)	36(1)	19(2)	4.4(4)	23(2)	−5(1)	−4(2)
O2	0.116(2)	0.879(2)	0.014(4)	4.1(9)	1(1)	20(2)	−1.0(6)	5.6(9)	−1(1)
O3	0.784(1)	0.208(2)	−0.021(4)	5.4(10)	1.8(7)	22(2)	1.6(8)	−7.5(10)	−4.3(8)
O4	0.450(1)	0.546(2)	0.012(4)	3.7(9)	1.1(7)	11.7(11)	1.3(6)	1.4(9)	−0.6(9)

Numbers in parentheses are standard deviations of last significant digits. Values with no standard deviation shown were not refined. Atomic thermal displacement parameters values are multiplied by 100.
[a]710 °C: $a = 8.9291(1)$ Å, $c = 8.4963(4)$ Å; $R_p = 3.15\%$, $R_{wp} = 2.29\%$, $\chi^2 = 3.56$.
[b]800 °C: $a = 8.9349(1)$ Å, $c = 8.5109(3)$ Å; $R_p = 2.58\%$, $R_{wp} = 1.93\%$, $\chi^2 = 3.46$.

with the maximum of extra nuclear scattering density located around (0.58, 0.16, 1/4). The refinement with the apical oxygen atoms located in the 6*h* (*x*,2*x*,1/4) split site resulted in a significant improvement of the refinement quality. The R_p, R_{wp}, and χ^2 values dropped from 3.44%, 2.50% and 4.48 to 2.90%, 2.29%, and 3.21, respectively. An attempt to introduce additional degrees of freedom for apical oxygen atoms by further splitting 6*h* site to the general 12*i* (*x*,*y*,*z*) type did not improve the refinement. As might be expected for a rigid tetrahedron unit, displacement of the apical oxygen atoms in the *ab*-plane affects the basal oxygen atoms, whose thermal ellipsoids were found to be significantly elongated along *c*-axis (Fig. 9b). These two interconnected effects, i.e. apical oxygen site splitting in the *ab*-plane and high anisotropy of thermal displacement of the basal oxygen atoms, seem to be a common feature of stuffed tridymite derivatives with the $P6_322$ space group as they were observed in analogues with various combinations of *A* and *M* elements, i.e. *A* = Ba, Sr, K/Ba and *M* = Al, Ga, Fe/Ge [16–19]. There arises a question whether high anisotropy of thermal ellipsoids of the basal oxygen atoms indicates that they also should be modeled by a split site. In fact, models with split sites for both apical and basal oxygen atoms were recently proposed for $P6_322$ aluminates $Sr_{0.864}Eu_{0.136}Al_2O_4$ [20] and $Ba_{0.6}Sr_{0.4}Al_2O_4$ [21] based on the maximum entropy method analysis of X-ray powder diffraction data. However, the refinement of our neutron diffraction data with the basal oxygen atoms located in the split 12*i* (*x*,*y*,*z*) site and isotropic thermal parameters degraded refinement quality resulting in the R_p, R_{wp}, and χ^2 values equal to 3.08%, 2.40%, and 3.61, respectively. The refinement of the model with the basal oxygen atoms in 12*i* (*x*,*y*,*z*) sites and anisotropic thermal parameters was not stable due to very high correlation between *z*-coordinate and U_{33} anisotropic thermal parameter tensor component. Therefore, both data sets collected at 1000 and 1200 °C were refined with the apical and basal oxygen atoms located in the split 6*h* (*x*,2*x*,1/4) and the ideal 6*g* (*x*,0,0) sites, respectively. The results are presented in Fig. 8. The crystallographic details are provided in Table 4.

3.3. Crystal chemistry of $P2_1$, $P6_3(\sqrt{3}A)$, and $P6_322$ phases of stuffed tridymites

There is a general agreement in literature that topology and a degree of deformation of the high tridymite type framework in AM_2O_4 derivatives is determined by the size of A^{n+} cations with respect to the size of cavities in the $[^2M_2O_4]^{n-}$ framework [13,22]. The cations Sr^{2+} are apparently too small for nine-fold coordination of the large cavities in the undistorted $[^2Al_2O_4]^{2-}$ framework and the structure at room temperature is severely collapsed to form irregular polyhedra with six Sr–O distances close to the sum of ionic radii [6]. On heating thermal expansion of *A* sites, higher than that of AlO_4 tetrahedra, drives the structure toward the ideal hexagonal symmetry and at 680 °C the structure transforms to $P6_3(\sqrt{3}A)$ form.

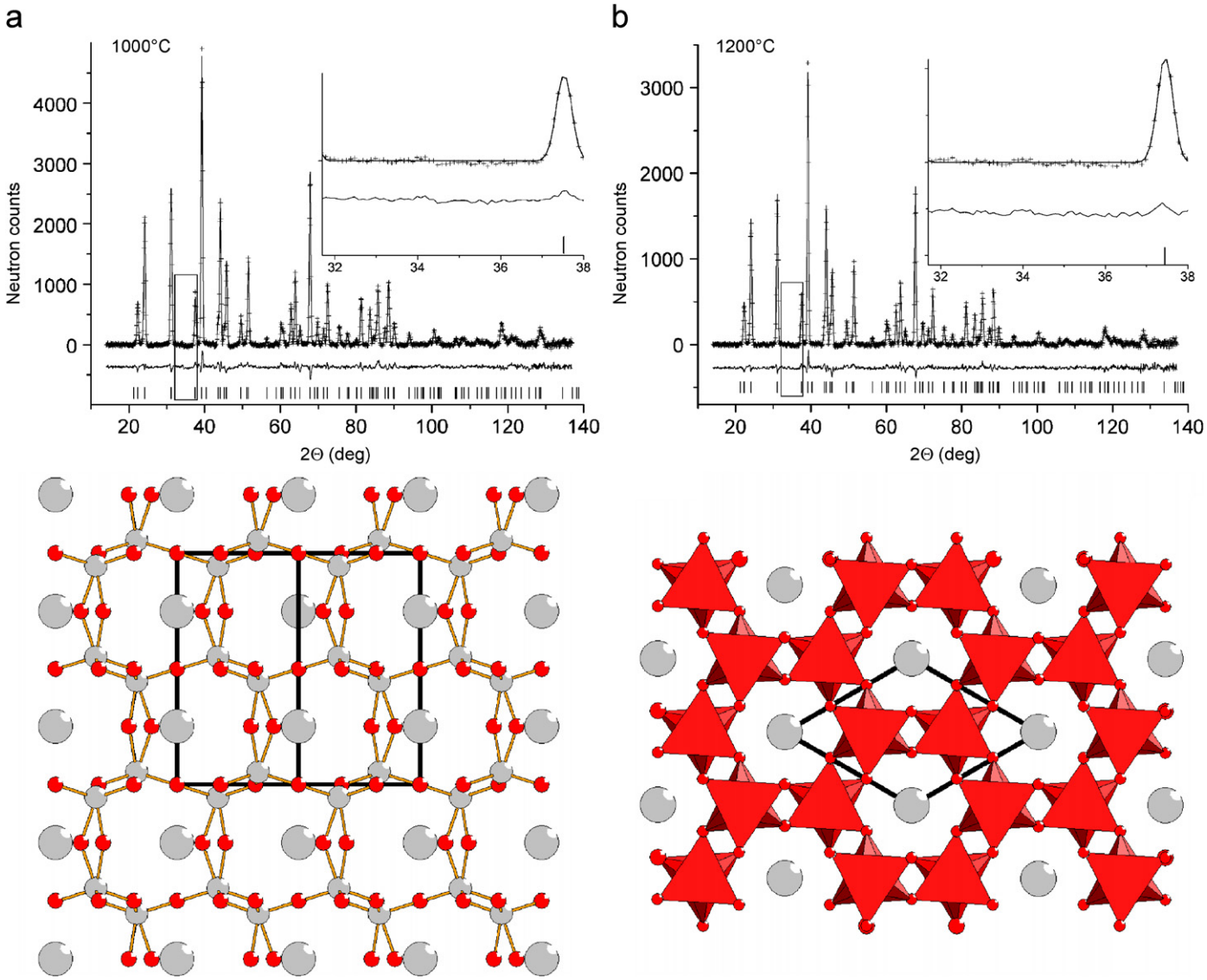

Fig. 8. Top: neutron powder diffraction observed and calculated profiles, and difference curves for the hexagonal $P6_322$ modification of $SrAl_2O_4$ at 1000 and 1200 °C. Inset shows the same characteristic region as in Fig. 6 to illustrate absence of $\sqrt{3}A$ superstructure reflections. Bottom: view of $P6_3$ modification of $SrAl_2O_4$ perpendicular (left) and parallel (right) to the hexagonal c-axis.

As has been pointed out before [15,23], the key feature of the $P6_3(\sqrt{3}A)$ superstructure with respect to the undistorted high tridymite framework is a displacement of the apical oxygen atoms in the basal plane from their ideal positions (Fig. 9a). This, obviously, results in decreasing the M–O^{apical}–M angle from 180° down to ~145–155° (Table 5) and in splitting of each atomic position to several symmetrically distinct sites. This splitting of (2*b*) and (4*f*) Wyckoff sites of the $P6_322$ space group to (2*a*) + (2*b*) + (2*b*) and (6*c*) + (6*c*) sites in $P6_3(\sqrt{3}A)$ space group for A and M cations, respectively, was suggested to favor the occurrence of the $P6_3(\sqrt{3}A)$ phase only in materials with *chemically* distinct cations occupying crystallographically inequivalent sites in ordered manner [15,23,24]. Indeed, this idea is clearly supported by the list of materials in which the $P6_3(\sqrt{3}A)$ phase was observed so far (Table 5). For all of them complete or partial cation order was reported. However, the example of $SrAl_2O_4$ with the only type of cations on both A and M sites, suggests that having more than one type of atoms on A and/or M site is not a necessary condition and the size mismatch of A cation and the cavity it occupies is sufficient for the formation of $P6_3(\sqrt{3}A)$ phase. Recently, an attempt was made to establish quantitative relations between the degree of framework distortion in stuffed tridymites and crystal chemical characteristics of cations in terms of the average $\langle M\text{–O–}M \rangle$ angle as a function of the difference between the average cation–oxygen interatomic distances $\langle A\text{–O} \rangle$-$\langle M\text{–O} \rangle$ [25]. As might be expected, the $\langle \text{O–}M\text{–O} \rangle$ angle was found to increase when the size mismatch decreases. However, based on the results of this study and literature data (Table 6) we argue that in $P6_322$ stuffed tridymites $\langle M\text{–O–}M \rangle$ never exceeds the same upper limit ~160° as in $P6_3(\sqrt{3}A)$ phases (Table 5) and

never reaches the ideal value 180°. Instead, $P6_322$ symmetry is gained by disordering off-center split sites of apical oxygen atoms around 3-fold axis (Fig. 9b). The only composition standing out in Table 6 is $BaZnGeO_4$ for which the (Zn,Ge)–O^{apical}–(Zn,Ge) angle is reported to have the ideal value 180°. However, we notice that for room temperature $P6_3(\sqrt{3}A)$ modification of $BaZnGeO_4$ the same authors report average $\langle Zn–O^{apical}\rangle$ and $\langle Ge–O^{apical}\rangle$ distances 1.88 and 1.75 Å, respectively [26] but for $P6_322$ modification at 900 °C (!) they find (Zn,Ge)–O^{apical} distance only 1.78 Å. We believe that O^{apical} site splitting has been overlooked and crystal structure of $BaZnGeO_4$ should be re-investigated.

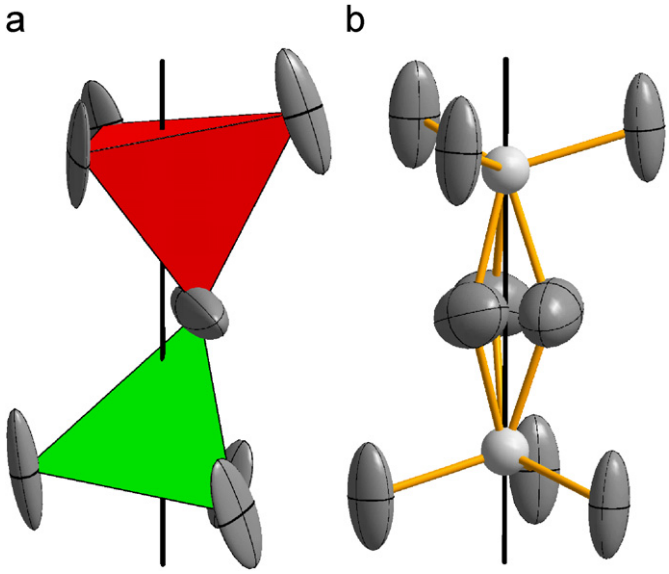

Fig. 9. Ordered (left) and disordered (right) off-center displacement of the apical oxygen atoms in $P6_3(\sqrt{3}A)$ and $P6_322$ modifications of $SrAl_2O_4$, respectively. Solid black line indicates the position of the 3-fold axis.

4. Conclusions

To clarify contradicting reports on symmetry of high-temperature phases of $SrAl_2O_4$, we investigated

Table 5
The M–O^{apical}–M angles for known $P6_3(\sqrt{3}A)$ structures

Composition	M–O^{apical}–M angle
$NaZnAsO_4$ [27] (14 K)[a]	127.6
$NaZnAsO_4$ [27] (298 K)[a]	127.8
$(Ba_{0.5}Sr_{0.5})Ga_2O_4$ [28][b]	132.9, 137.7
$BaZnGeO_4$, RT [26]	138.4, 167.2, 138.8
$NaGaSiO_4$ [29]	139.1
$NaBSiO_4$ [30]	140.7
$Na_{0.7}K_{0.3}GaSiO_4$ [24]	144.1
$SrAl_2O_4$, 800 °C [8]	147.4
$BaCoSiO_4$ [15]	148.6
$BaMgSiO_4$ [15]	157.1
$BaZnSiO_4$ [15]	157.2
$SrAl_2O_4$, 710 °C (this work)	153.8(9)
$SrAl_2O_4$, 800 °C (this work)	152.0(7)

[a]Prepared by soft dehydration of $Na_6(ZnAsO_4)_6 \cdot 8H_2O$ under vacuum and is probably metastable.
[b]Described with two-fold split apical oxygen site.

Table 6
The M–O^{apical}–M angles for known $P6_322$ structures

Composition	M–O^{apical}–M angle
$Sr_{0.864}Eu_{0.136}Al_2O_4$ [20]	136.2
$K_{0.75}Ba_{0.25}Fe_{1.25}Ge_{0.75}O_4$ [19]	142.9
β-$BaGa_2O_4$ [18]	144.9
$Ba_{0.6}Sr_{0.4}Al_2O_4$ [21]	147.3
$BaAlGaO_4$ [17]	151.3
$BaAl_2O_4$ [16]	157.6
$BaZnGeO_4$, 900 °C [31]	180
$SrAl_2O_4$, 1000 °C (this work)	142.9(3)
$SrAl_2O_4$, 1200 °C (this work)	143.8(3)

Table 4
Structural parameters for $SrAl_2O_4$ refined from neutron powder diffraction data collected at 1000 and 1200 °C using hexagonal space group $P6_322$ (No. 182) with Sr1 at $2b$(0,0,1/4), Al1 at $4f$(1/3,2/3,z), O1 at $6h$(x,2x,1/4), and O4 at $6g$(x,0,0)

Atom	x	y	z	U_{11}, Å^2	U_{22}, Å^2	U_{33}, Å^2	U_{12}, Å^2	U_{13}, Å^2	U_{23}, Å^2
				1000 °C[a]					
Sr1	0	0	1/4	4.2(1)	$=U_{11}$	6.2(2)	2.1(1)	0	0
Al1	1/3	2/3	0.9457(3)			$U_{iso}=3.5(1)$			
O1[c]	0.6039(5)	0.2077(10)	1/4	9.7(4)	6.0(5)	6.7(4)	3.0(2)	1.2(7)	0
O2	0.3574(3)	0	0	3.6(1)	2.5(1)	17.5(2)	1.2(1)	−0.5(1)	−0.9(2)
				1200 °C[b]					
Sr1	0	0	1/4	5.0(1)	$=U_{11}$	7.1(3)	2.5(1)	0	0
Al1	1/3	2/3	0.9451(3)			$U_{iso}=4.0(1)$			
O1[c]	0.6057(6)	0.2114(12)	1/4	10.3(5)	6.7(6)	6.4(4)	3.4(3)	1.5(8)	0
O2	0.3591(4)	0	0	4.1(1)	3.0(1)	18.5(2)	1.5(1)	−0.9(1)	−1.8(2)

Numbers in parentheses are standard deviations of last significant digits. Values with no standard deviation shown were not refined. Atomic thermal displacement parameters values are multiplied by 100.
[a]1000 °C: $a=5.1666(1)$ Å, $c=8.5485(3)$ Å; $R_p=2.90\%$, $R_{wp}=2.29\%$, $\chi^2=3.21$.
[b]1200 °C: $a=5.1765(1)$ Å, $c=8.5758(1)$ Å; $R_p=2.95\%$, $R_{wp}=2.38\%$, $\chi^2=2.27$.
[c]Site occupancy factor is 1/3.

temperature evolution of its crystal structure using X-ray and neutron powder diffraction. The previously reported first order monoclinic↔hexagonal phase transition at ~680 °C was confirmed but the correct space group of $SrAl_2O_4$ above the transition is $P6_3$ rather than $P6_322$. Lower than previously reported symmetry originates from ordered displacement in the *ab*-plane of apical oxygen atoms linking tridymite type layers. On further heating $SrAl_2O_4$ undergoes a second-order transition to $P6_322$ modification at ~860 °C. However, higher symmetry is gained by disorder of off-center displaced apical oxygen atoms around 3-fold axis rather than by eliminating displacements. The analysis of crystallographic data for isostructural analogues AM_2O_4 (A = Ba, K/Ba, Sr/Eu; M = Al, Ga, Fe/Ge) suggests that it is a common feature of $P6_322$ phases of stuffed tridymites.

Acknowledgments

This work was partially supported by the FCT, Portugal (projects POCI/CTM/58570/2004 and PTDC/CTM/64357/2006). MA is grateful to the powder diffraction team and technical staff of the Bragg Institute for the help during the Echidna diffractometer commissioning.

References

[1] S.H.M. Poort, W.P. Blokpoel, G. Blasse, Chem. Mater. 7 (1995) 1547.
[2] A.A. Yaremchenko, V.V. Kharton, A.L. Shaula, F.M.M. Snijkers, J.F.C. Cooymans, J.J. Luyten, F.M.B. Marques, J. Electrochem. Soc. 153 (2006) J50.
[3] A.A. Yaremchenko, V.V. Kharton, M. Avdeev, A.L. Shaula, F.M.B. Marques, Solid State Ionics 178 (2007) 1205.
[4] H. Müller-Buschbaum, J. Alloy Compds. 349 (2003) 49.
[5] S. Ito, S. Banno, K. Suzuki, M. Inagaki, Z. Phys. Chem. Neue Folge 105 (1977) 173.
[6] A.-R. Schulze, H.K. Müller-Buschbaum, Z. Anorg. Allg. Chem. 475 (1981) 205.
[7] U. Rodehorst, M.A. Carpenter, S. Marion, C.M.B. Henderson, Mineral Magn. 67 (2003) 989.
[8] K. Fukuda, K. Fukushima, J. Solid State Chem. 178 (2005) 2709.
[9] L.A. Chick, L.R. Pederson, G.D. Maupin, J.L. Bates, L.E. Thomas, G.J. Exarhos, Mater. Lett. 10 (1990) 6.
[10] A.C. Larson, R.B. Von Dreele, Los Alamos National Laboratory Report LAUR 86-748, 2004.
[11] B.H. Toby, J. Appl. Crystallogr. 34 (2001) 210.
[12] ICDD, International Center for Diffraction Data, 12 Campus Boulevard, Newton Square, Pennsylvania 19073-3273, USA.
[13] C.M.B. Henderson, D. Taylor, Mineral Magn. 45 (1982) 111.
[14] M.I. Aroyo, J.M. Perez-Mato, C. Capillas, E. Kroumova, S. Ivantchev, G. Madariaga, A. Kirov, H. Wondratschek, Z. Kristallogr. 221 (2006) 15.
[15] B. Liu, J. Barbier, J. Solid State Chem. 102 (1993) 115.
[16] A.J. Perrotta, J.V. Smith, Bull. Soc. Fr. Mineral Cristallogr. 91 (1968) 85.
[17] V. Kahlenberg, J.B. Parise, Y. Lee, A. Tripathi, Z. Kristallogr. 217 (2002) 249.
[18] V. Kahlenberg, C. Weidenthaler, Solid State Sci. 4 (2002) 963.
[19] J. Choisnet, V. Caignaert, B. Raveau, J. Mater. Chem. 14 (2004) 2438.
[20] H. Yamada, W.S. Shi, C.N. Xu, J. Appl. Crystallogr. 37 (2004) 698.
[21] K. Fukuda, T. Iwata, T. Orito, J. Solid State Chem. 178 (2005) 3662.
[22] J. Barbier, M.E. Fleet, Phys. Chem. Minerals 16 (1988) 276.
[23] M.A. Carpenter, D. Cellai, Am. Mineral 81 (1996) 561.
[24] J. Barbier, B. Liu, J. Weber, Eur. J. Mineral 5 (1993) 297.
[25] H. Lemmens, S. Amelinckx, G. Van Tendeloo, A.M. Abakumov, M.G. Rozova, E.V. Antipov, Phase Transit. 76 (2003) 653.
[26] K. Iijima, F. Marumo, H. Takei, Acta Crystallogr. Sec. B 38 (1982) 1112.
[27] T.M. Nenoff, W.T.A. Harrison, G.D. Stucky, J.M. Nicol, J.M. Newsam, Zeolites 13 (1993) 506.
[28] S. Kubota, T. Takahashi, H. Yamane, M. Shimada, J. Alloys Compds. 345 (2002) 105.
[29] T.M. Gesing, Z. Kristallogr. 215 (2000) 510.
[30] Y.V. Sokolova, A.P. Khomyakov, Doklady Akademii Nauk Sssr 319 (1991) 879.
[31] K. Iijima, F. Marumo, H. Takei, J. Ceram Assoc. Japan 91 (1983) 67.